Detecting causality based on state space reconstruction from interspike intervals for neural spike trains

Kazuya Sawada [*]
Department of Information and Computer Technology, Faculty of Engineering, Tokyo University of Science, Niijuku 6–3–1, Katsushika-ku, Tokyo 125–8585, Japan

Yutaka Shimada [†]
Department of Information and Computer Sciences, Graduate School of Science and Engineering, Saitama University, 255 Shimo-Okubo, Sakura-ku, Saitama-shi, Saitama 338–8570, Japan

Tohru Ikeguchi [‡]
Department of Information and Computer Technology, Faculty of Engineering, Tokyo University of Science, Niijuku 6–3–1, Katsushika-ku, Tokyo 125—8585, Japan

(Received 25 August 2023; revised 22 May 2025; accepted 6 June 2025; published 28 July 2025)

System analysis depends critically on the identification of the connections—especially the causal relationships—that exist between the components of the system. In particular, the causal relationships connecting neurons in brains, whose activities are typically observed as spike trains (a type of point process), need to be elucidated. Although various causality detection methods have been developed for time series signals, an effective causality detection method for spike trains has not been developed yet. To this end, we propose a causality detection method for spike trains based on the theory of nonlinear dynamical systems. We use the mutual prediction accuracy of the interspike intervals of spike trains for causality detection. Furthermore, we test the prediction accuracy obtained by the proposed method using the method of surrogate data from nonlinear dynamical systems theory. Numerical experiments revealed that the proposed method provides accurate causality detection for a small number of neural spike trains generated by the mathematical model.

DOI: 10.1103/t2jb-vvx9

I. INTRODUCTION

The development of a highly accurate method for detecting causality, using only time series data, is critical for numerous applications. Causality detection methods have been used to investigate the dynamics of complex systems, such as economic activities, natural phenomena, neural activities, and gene regulatory networks [1–3]. Furthermore, certain causality detection methods have been applied to estimate a network structure, and several studies have focused on the relationship between the accuracy of the causality detection and the network structure [4,5] because the accuracy of the causality detection depends on the network structure.

The Granger causality (GC) [6] and transfer entropy (TE) [7] are widely used to detect causality. However, various caveats apply to these methods. For example, GC requires constructing an appropriate predictor, which means that GC is not model-free. Furthermore, the independence of variables is crucial in causality detection when using the GC, and the normality of the time series data and the linearity of causality are assumed. Therefore, GC may not be effective for systems with nonlinear causalities, such as nonlinear dynamical systems, which are ubiquitous in the real world [8]. TE is a powerful method for detecting causality that is based on information theory and requires neither the normality of time series data nor the linearity of causality. However, TE requires a considerable amount of data for calculating probability distributions, and the computation time is high when a delay occurs in causality.

To solve these problems, a method called convergent cross mapping (CCM) [8] has been proposed to detect causality even for small volume datasets obtained from nonlinear dynamical systems. CCM is a causality detection method based on nonlinear dynamical systems theory, in which state space reconstruction is performed using time series data [9,10] to detect causality using the in-sample mutual-prediction accuracy. CCM is a highly useful method for a wide variety of nonlinear deterministic dynamical systems without specific restrictions. Importantly, CCM can distinguish real causality from spurious causality. In addition to CCM, cross-map smoothness (CMS) [3] and partial cross mapping (PCM) [11] have been proposed as extended causality detection methods that reconstruct the state space and utilize the mutual prediction.

[*]Contact author: sawada@hisenkei.net
[†]Contact author: yshimada@mail.saitama-u.ac.jp
[‡]Contact author: tohru@rs.tus.ac.jp

Published by the American Physical Society under the terms of the Creative Commons Attribution 4.0 International license. Further distribution of this work must maintain attribution to the author(s) and the published article's title, journal citation, and DOI.

The aforementioned methods can be applied to time series data with a regular sampling interval, but not directly to point processes with irregular sampling intervals. However, point processes are ubiquitous in daily life; typical examples of point processes include neural activities, seismic activities, and price movements in financial markets [12–15]. For example, extreme rainfall events in climate data can be treated as point process data, and causality detection methods have been applied to such data to detect causal paths among factors of climate change and to estimate networks [16–18]. Although several methods have been proposed for estimating the network structure and detecting causality from point process data [19–23], the foundations of causality analysis methods for point processes, especially those for point processes generated by nonlinear dynamical systems, have not been sufficiently developed.

Therefore, in this study, we developed a causality detection method for point processes, especially for neural spike trains, by modifying the CCM framework to detect causality for point processes. In the modification of CCM, we addressed two issues. The first issue is to reconstruct the state space only from the point process. To resolve this issue, we used the technique of state space reconstruction from the interspike intervals (ISIs) of spike trains [24–27], where a state space can be reconstructed by converting an ISI time series into a time-delay coordinate system. The second issue is to establish a temporal correspondence between the state values of two ISI time series. The original CCM detects causal relations by in-sample mutual prediction using the information of the reconstructed state space, in which the temporal correspondence between the time-delay vectors in the reconstructed state space is required. Similarly, when modifying the CCM for point processes, it is necessary to establish the temporal correspondence between the time-delay ISI vectors on the reconstructed state space. However, this task is not straightforward because ISI time series do not include precise temporal information. In order to address this issue, we proposed a technique to establish the temporal correspondence between ISI time series. By combining the two aforementioned techniques, we developed a causality detection method for neural spike trains by applying CCM to the ISIs of spike trains. Subsequently, we applied the proposed method to spike trains generated from a mathematical model with causality, in order to verify the effectiveness of the proposed method. A further important aspect of this study was the use of twin surrogate data of ISI time series when determining the presence or absence of causality based on the in-sample prediction accuracies in the modified CCM framework.

In summary, the contribution of this study is twofold: (i) the proposal of a causality detection method for spike trains that modifies the CCM using two techniques: reconstructing dynamical systems only from the ISI time series, and establishing the temporal correspondence between two ISI time series; (ii) the proposal of a method for assessing the statistical significance of prediction accuracy using twin surrogate data of ISI time series, thus ascertaining the presence or absence of causality.

The remainder of this paper is organized as follows. Section II presents a review of the original CCM method. Additionally, the proposed method for detecting causality for neural spike trains is described, and a significance test using the twin surrogate method is stated. In Sec. III, the results of the numerical experiments are detailed, and in Sec. IV, the conclusions drawn from the study are presented, and a few selected problems and the limitations of the proposed method are discussed.

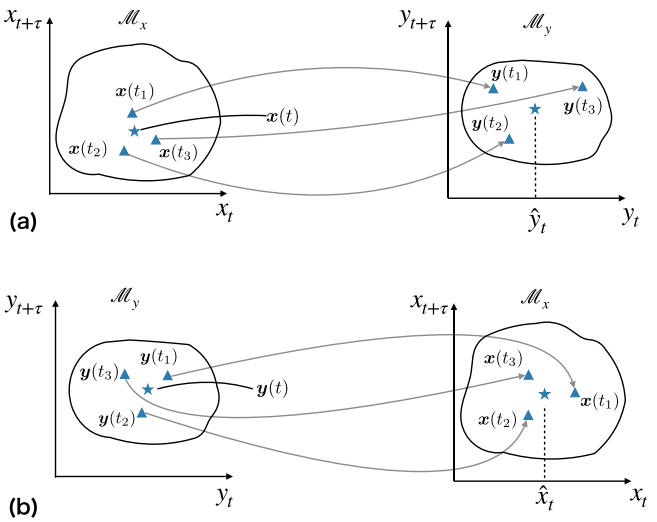


FIG. 1. Basic concept of cross mapping in CCM. (a) Prediction of y_t by using the neighborhood information of $\boldsymbol{x}(t)$ on manifold $\mathcal{M}_x$, (b) Prediction of x_t by using the neighborhood information of $\boldsymbol{y}(t)$ on manifold $\mathcal{M}_y$. The predicted values of x_t and y_t are $\hat{x}_t$ and $\hat{y}_t$, where $\hat{x}_t$ and $\hat{y}_t$ are the weighted center of gravity of $\boldsymbol{x}(t_i)$ and $\boldsymbol{y}(t_i)$ $(i = 1 \sim 3)$. $\boldsymbol{x}(t_i)$ and $\boldsymbol{y}(t_i)$ are the i-th neighboring points of $\boldsymbol{x}(t)$ and $\boldsymbol{y}(t)$.

II. METHODS

A. Overview of CCM

CCM is used for detecting causality based on nonlinear dynamical systems theory. In particular, this method is used to detect causality based on the accuracy of in-sample mutual predictions for two observed time series. In CCM, the reconstructed state space through the delay-coordinate system [9,10] is utilized. For example, if two time series x_t and y_t are observed, their time-delay vectors are defined as Eqs. (1) and (2):

$$\boldsymbol{x}(t) = (x_t, x_{t+\tau}, x_{t+2\tau}, \ldots, x_{t+(D-1)\tau}), \tag{1}$$

$$\boldsymbol{y}(t) = (y_t, y_{t+\tau}, y_{t+2\tau}, \ldots, y_{t+(D-1)\tau}), \tag{2}$$

where D is the reconstruction dimension and τ is the time delay. Critical components of CCM are in-sample mutual predictions using cross mapping, and convergence of the prediction accuracy as the time series length increases. Moreover, predictions using cross mapping require knowledge of the temporal correspondence between neighboring points on the reconstructed state spaces from two observed time series. The basic concept of cross mapping in CCM is illustrated in Fig. 1. A causal relationship is assumed from variable x to variable y. Thus, this case may be expressed by the following mathematical relationship between variables x and y: $x_{t+1} = f(x_t)$ and $y_{t+1} =$

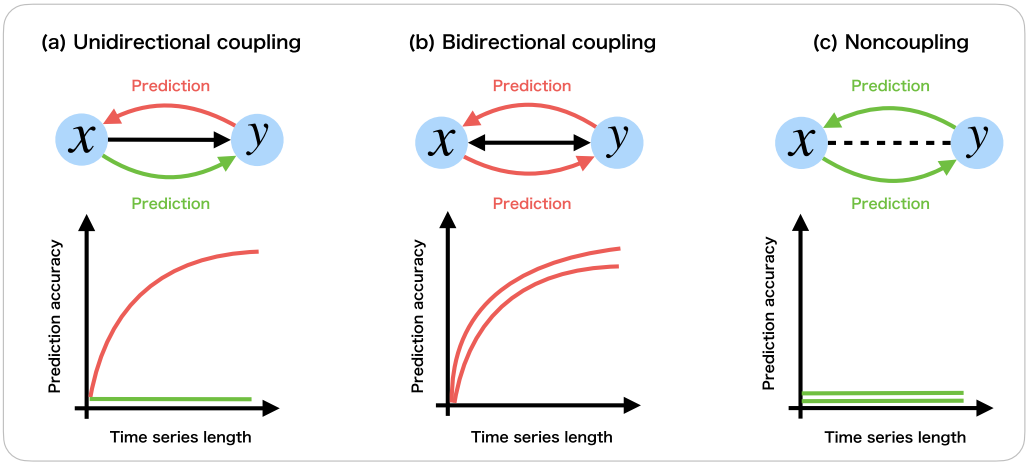


FIG. 2. Relationships between the causal patterns and the transitions of prediction accuracies with increasing time series length used for prediction. (a) Unidirectional coupling case: x is a driving variable (causing variable) and y is a driven variable (resulting variable), that is, causal direction is $x \to y$. (b) Bidirectional coupling case: x and y are driving and driven variables (causing and resulting variables), that is, causal directions are $x \leftrightarrow y$. (c) Noncoupling case: When we predict the causing variables by using the resulting variables, the prediction accuracies converge to higher values as the time series length used for prediction increases (red lines). By contrast, when we predict the resulting variables by using causing variables, the prediction accuracies converge to lower values as the time series length used for prediction increases (green lines).

$g(x_t, y_t)$. In Fig. 1, $\mathcal{M}_x$ and $\mathcal{M}_y$ represent manifolds reconstructed from the time series x_t and y_t, respectively. Figure 1(a) displays the case in which we predict y_t by using the information in the reconstructed state space of x_t, namely $\mathcal{M}_x$; Fig. 1(b) displays the case in which we predict x_t by using the information in the reconstructed state space of y_t, namely, $\mathcal{M}_y$. Here, we define the i-th neighboring point of $\boldsymbol{x}(t)$ and $\boldsymbol{y}(t)$ as $\boldsymbol{x}(t_i)$ and $\boldsymbol{y}(t_i)$. When predicting state value y_t by using the information on $\mathcal{M}_x$, we first determine the neighborhood of the time-delay vector $\boldsymbol{x}(t)$ on $\mathcal{M}_x$, namely, $\boldsymbol{x}(t_i)$. In this example, we set the number of neighboring points as three, namely $\boldsymbol{x}(t_i)$ $(i = 1 \sim 3)$, because we show a schematic illustration with a two-dimensional reconstructed state space in Fig. 1. Subsequently, we set the predicted value $\hat{y}_t$ as the center of gravity of $\boldsymbol{y}(t_i)$ $(i = 1 \sim 3)$. In this case, the prediction accuracy about $\hat{y}_t$ is likely to be low because variable x causes variable y, that is, variable x is not controlled by variable y and does not include the information of variable y. By contrast, the prediction accuracy about $\hat{x}_t$ by using information on $\mathcal{M}_y$ is likely to be high because variable x causes variable y, that is, variable y is controlled by variable x and includes the information of variable x. Thus, if $\boldsymbol{y}(t_i)$ $(i = 1 \sim 3)$ are determined as the neighboring points of $\boldsymbol{y}(t)$, $\boldsymbol{x}(t_i)$ $(i = 1 \sim 3)$, which temporally correspond to $\boldsymbol{y}(t_i)$ $(i = 1 \sim 3)$, are likely to be neighboring points of $\boldsymbol{x}(t)$ [Fig. 1(b)].

In CCM, the causality can be detected using these characteristics. In particular, as displayed in Fig. 2, the convergence of the prediction accuracy in cross mapping determines the existence and direction of causality. As shown in Fig. 2, in the case of predicting the causing variable by using the resulting variable (red lines), the prediction accuracies converge to higher values as the time series length used for prediction increases. By contrast, when predicting the resulting variable by using the causing variable (green lines), the prediction accuracies converge to lower values as the time series length used for prediction increases. Thus, CCM can detect causality.

B. Proposed method for detecting causality in spike trains

CCM is an effective method for detecting causality between different sets of nonlinear deterministic time series data. However, in this capacity, CCM is applied to time series data with regular sampling intervals and cannot be applied to point processes such as spike trains, which have irregular sampling intervals. Consequently, we propose a modification for CCM, enabling the detection of causality between spike trains. Now, for simplicity, we consider the case of observing two spike trains as displayed in Fig. 3.When we define the n-th firing time of the i-th neuron as $S_i(n)$, the n-th ISI of the i-th neuron is defined by $T_i(n) = S_i(n+1) - S_i(n)$, as displayed in Fig. 3. Even when the sampling intervals of time series are irregular, the state space can be reconstructed from the ISI time series by generating time-delay vectors, expressed as

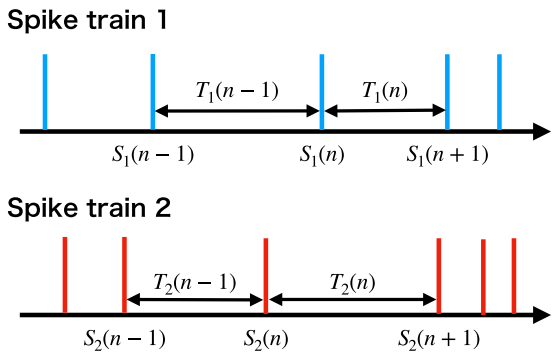


FIG. 3. An example of two observed spike trains. $S_i(n)$ and $T_i(n)$ are the n-th firing time and interspike interval (ISI), respectively, of the i-th neuron $(i = 1,\ 2)$.

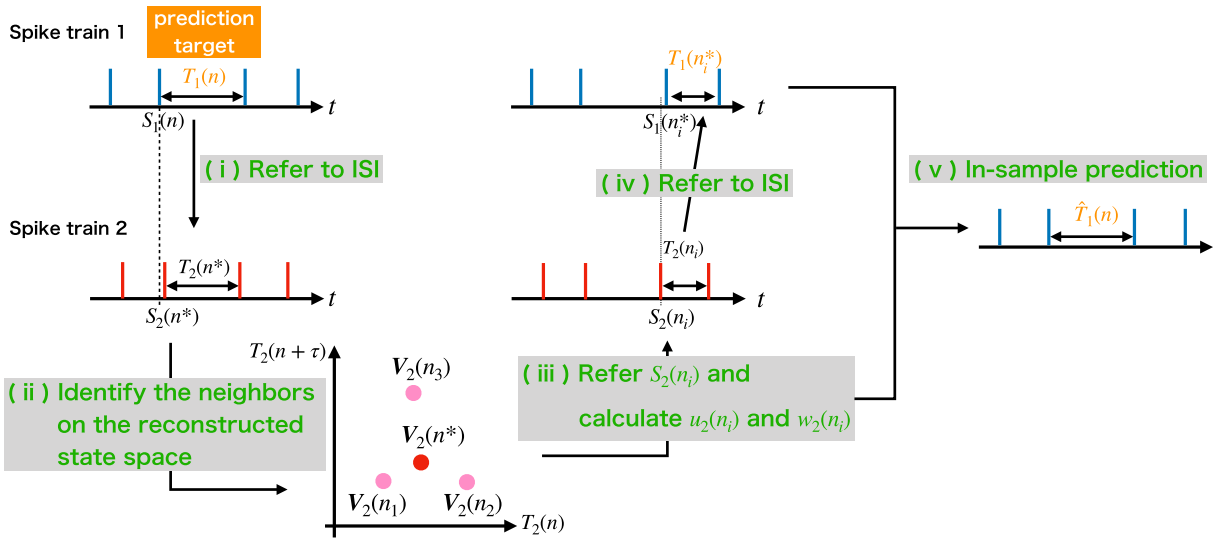


FIG. 4. In-sample prediction flow for spike trains used for the proposed method.

follows in Eq. (3) [24–27]:

$$\boldsymbol{V}_i(n) = (T_i(n), T_i(n+\tau), \ldots, T_i(n+(D-1)\tau)), \quad (3)$$

where τ is the time delay and D is the reconstruction dimension. Using the above definition of the ISI and Eq. (3), a dynamical system can be reconstructed from ISI time series [24–27]. Next, we mutually predict the ISI time series based on the information of neighbors in the state space reconstructed from the ISI time series, in accordance with the CCM framework. Although we have only described the prediction of the ISI of spike train 1, $T_1(n)$, by using $T_2(n)$, the same procedure applies to the prediction of $T_2(n)$ by using $T_1(n)$. To perform the prediction, we first define $\hat{T}_1(n)$ as the predicted time series of $T_1(n)$. $\hat{T}_1(n)$ is calculated as follows:

$$\hat{T}_1(n) = \sum_{i=1}^{K} w_2(n_i) T_1(n_i^*), \quad (4)$$

where n_i is the index of the i-th nearest neighboring point for the reconstructed vector of the index n^* in the reconstructed state space. Moreover, $w_2(n_i)$ is the weight calculated from the i-th nearest neighbor of the time-delay vector $\boldsymbol{V}_2(n^*)$ in the reconstructed state space. The meaning of * is explained in Eq. (8). In Eq. (4), K is the number of neighbors used for predicting the ISI time series. In the numerical experiments, we used $K = D + 1$, similar to the original CCM algorithm. The weight $w_2(n_i)$ is defined as follows:

$$w_2(n_i) = \frac{u_2(n_i)}{\sum_{j=1}^{K} u_2(n_j)}. \quad (5)$$

In Eq. (5), $u_2(n_i)$ is defined as follows:

$$u_2(n_i) = \exp\left\{\frac{-d[\boldsymbol{V}_2(n^*), \boldsymbol{V}_2(n_i)]}{d[\boldsymbol{V}_2(n^*), \boldsymbol{V}_2(n_1)]}\right\}, \quad (6)$$

where $d[\boldsymbol{V}_2(n^*), \boldsymbol{V}_2(n_i)]$ is the Euclidean distance between $\boldsymbol{V}_2(n^*)$ and $\boldsymbol{V}_2(n_i)$. $\boldsymbol{V}_2(n_i)$ is the i-th nearest neighbor of $\boldsymbol{V}_2(n^*)$ in the reconstructed state space. If $d[\boldsymbol{V}_2(n^*), \boldsymbol{V}_2(n_1)] = 0$, then $u_2(n_i)$ is defined as follows:

$$u_2(n_i) = \begin{cases} 1 & (i = 1), \\ 0 & (i \neq 1). \end{cases} \quad (7)$$

We summarize the in-sample mutual prediction flow used for the proposed method in Fig. 4. As displayed in Fig. 4, we first consider the case in which we predict $T_1(n)$ using $T_2(n)$. The prediction steps (i)∼(v) are as follows:

(i) To predict $T_1(n)$, we refer to the ISI $T_2(n^*)$, which corresponds to $S_2(n^*)$, the nearest spike timing to $S_1(n)$. n^* is calculated using Eq. (8).

$$n^* \in \underset{n'}{\operatorname{argmin}} |S_2(n') - S_1(n)|. \quad (8)$$

Thus, n^* is the index number of that specific ISI on spike train 2 whose spike timing is the nearest to $S_1(n)$ on spike train 1.

(ii) We identify the i-th nearest neighbor of $\boldsymbol{V}_2(n^*)$, denoted by $\boldsymbol{V}_2(n_i)$, on the reconstructed state space.

(iii) Using Eqs. (5)–(7), we calculate $u_2(n_i)$ and $w_2(n_i)$. We refer to the spike timing $S_2(n_i)$ on spike train 2, which corresponds to the time of the i-th nearest neighbor of $\boldsymbol{V}_2(n^*)$.

(iv) We refer to the ISI $T_1(n_i^*)$ that corresponds to the spike with the nearest timing of $S_2(n_i)$. n_i^* is calculated using Eq. (9):

$$n_i^* \in \underset{n_i'}{\operatorname{argmin}} |S_1(n_i') - S_2(n_i)|. \quad (9)$$

(v) We calculate the weighted average of $T_1(n_i^*)$ referenced by step (iv) using the weight $w_2(n_i)$ calculated in step (iii). We predict $T_1(n)$ using Eq. (4).

The aforementioned procedures were implemented for all spikes to generate a predicted time series of the ISIs. The prediction accuracy was evaluated by the correlation coefficient $\rho[T_1|T_2]$ in the same way as Ref. [8]: $\rho[T_1|T_2]$ is the correlation coefficient between the actual time series $T_1(n)$ and the predicted time series $\hat{T}_1(n)$ obtained by Eq. (4). Then,

$\rho[T_1|T_2]$ is defined as follows:

$$\rho[T_1|T_2] = \frac{\sum_{n=1}^{T}(\hat{T}_1(n) - \bar{\hat{T}}_1)(T_1(n) - \bar{T}_1)}{\sqrt{\sum_{n=1}^{T}(\hat{T}_1(n) - \bar{\hat{T}}_1)^2}\sqrt{\sum_{n=1}^{T}(T_1(n) - \bar{T}_1)^2}}, \tag{10}$$

where T is the data length, $\bar{T}_1$ is the average of $T_1(n)$, and $\bar{\hat{T}}_1$ is the average of $\hat{T}_1(n)$. When the spike trains have causality and the time series data are sufficiently long, the prediction accuracy of the ISI time series increases and converges. The causality can be detected using this characteristic; that is, the proposed method is expected to work well for detecting causality for nonlinear deterministic dynamical systems because the proposed method is based on the embedding theorem through the time-delay coordinate system [9,10].

C. Significance test with twin surrogate data

The statistical significance of the prediction accuracy obtained by cross mapping is a critical criterion for the reliability of causality detection. Generally, the method of surrogate data is used for evaluating statistical significance testing in nonlinear time series analysis. Although various types of surrogate data methods have been proposed, the selection of the method depends on the specific index to be tested. The twin surrogate (TS) method [28] was used in this study because it is suitable for causality detection using CCM [29]. The TS method destroys only temporal relations, without losing the nonlinear properties of trajectories on the attractor, and generates alternative data based on the recurrence plot (RP) [30,31]. The TS data are generated as follows:

(i) Create an RP from the obtained time series. The RP is defined as follows: $R_{i,j} = \Theta(\delta - |\boldsymbol{x}(i) - \boldsymbol{x}(j)|)$, where $R_{i,j}$ is the $(i,\ j)$ pixel on the RP, Θ is the Heaviside function, δ is a threshold, $|\boldsymbol{x}(i) - \boldsymbol{x}(j)|$ is the Euclidean distance between $\boldsymbol{x}(i)$ and $\boldsymbol{x}(j)$, and $\boldsymbol{x}(i)$ is the i-th vector reconstructed from the obtained time series. In this study, we set $D = 5$ when reconstructing the attractor for an RP. The value of δ is calculated as follows: $\delta = r(Q_{\max} - Q_{\min}) + Q_{\min}$, where $Q_{\max}$ and $Q_{\min}$ are the maximum and minimum distances, respectively, between the time-delay vectors on the attractor, and r is a parameter that determines the threshold. In this study, we set $r = 0.1$.

(ii) Identify the "twin" on the created RP: $\boldsymbol{x}(i)$ and $\boldsymbol{x}(j)$ are defined as "twins" if they satisfy $R_{i,k} = R_{j,k}$ for all the values of k ($k = 1,\ 2,\ \ldots,\ T$). The TS method shuffles twins so that they become indistinguishable on the RP and shuffles the reconstructed vectors correspondingly by the following procedures, (iii)∼(vi).

(iii) Choose a starting point of the s-th TS data, $\boldsymbol{x}^s(1)$. The starting point $\boldsymbol{x}^s(1)$ is randomly selected from $\boldsymbol{x}(1), \boldsymbol{x}(2), \ldots, \boldsymbol{x}(T)$. Let l be the index of the starting point, that is, $\boldsymbol{x}^s(1) = \boldsymbol{x}(l)$ ($l \in \{1, 2, \ldots,\ T\}$). In the following steps, we determine $\boldsymbol{x}^s(2), \ldots, \boldsymbol{x}^s(T)$. We set $j = 1$.

(iv) If $\boldsymbol{x}(m)(m \in \{1, 2, \ldots,\ T-1\})$ is adopted as the j-th point of the s-th TS data, that is, $\boldsymbol{x}^s(j) = \boldsymbol{x}(m)$, and if $\boldsymbol{x}(m)$ has twins, we then set $\boldsymbol{x}^s(j+1)$ to one of the reconstructed state vectors selected from $\boldsymbol{x}(m+1), \boldsymbol{x}(m_1+1), \boldsymbol{x}(m_2+1), \ldots, \boldsymbol{x}(m_p+1)$ with equal probability, where p is the number of twins of $\boldsymbol{x}(m)$ and m_i is the i-th twin of $\boldsymbol{x}(m)$. However, if $\boldsymbol{x}^s(j) = \boldsymbol{x}(m)$ and $\boldsymbol{x}(m)$ does not have twins, we set $\boldsymbol{x}^s(j+1)$ to $\boldsymbol{x}(m+1)$.

(v) Increase j by $j \leftarrow j + 1$.

(vi) Iterate steps (iv)∼(v).

In step (iv), if $\boldsymbol{x}(T)$ is selected as $\boldsymbol{x}^s(j+1)$, we set $\boldsymbol{x}^s(j+2) = \boldsymbol{x}(q)$ to avoid cycling near the last value [32], where q is the index of the nearest vector of the terminal vector $\boldsymbol{x}(T)$, which is located in the first half of the trajectory of the attractor. Therefore, the index q is calculated using the following equation: $\min_q\ |\boldsymbol{x}(q) - \boldsymbol{x}(T)|(q \in [1, T/2])$. In other words, if the selected vector is the terminal vector during the process of generating surrogate data, we exceptionally conduct the transition from the terminal vector to the nearest neighbor vector of the terminal vector, which is selected in the first half of the trajectory of the attractor. The reason for this operation is that if the selected vector is the terminal vector during the process of generating surrogate data, and some of the vectors before the terminal vector are twins of the terminal vector, a cycle will occur near the terminal vector. This operation makes it possible to prevent a periodic cycle when the selected vector is the terminal vector during the generation of surrogate data, and the terminal vector has a twin. In addition, it is possible to generate surrogate data of the desired length even when the terminal vector does not have a twin.

When generating surrogate data using the TS method, if the number of twins is small, the same surrogate data may be generated. If the same surrogate data is included, the reliability of causality detection decreases. In the numerical experiments, we confirmed that there were no duplicates in the surrogate data generated (see Sec. III in Supplemental Material [33]).

III. RESULTS

The effectiveness of the proposed method was evaluated by applying it to two spike trains obtained using the Izhikevich neuron model [34] with a gap junction [35]. Two types of connections exist between neurons: chemical synaptic connections and electrical synaptic connections. In this study, the neurons were connected by a gap junction, which is the electrical synaptic connection. The response of the i-th Izhikevich neuron [35] coupled by a gap junction can be defined using the following equation:

$$\begin{aligned} \dot{\varphi}_i &= 0.04{\varphi_i}^2 + 5\varphi_i + 140 - \psi_i + I_i + \xi \\ &\quad + \sum_{i \neq j,\, j=0}^{M-1} \lambda_{ij}(\varphi_j - \varphi_i), \\ \dot{\psi}_i &= a_i(b_i\varphi_i - \psi_i), \end{aligned} \tag{11}$$

where $\varphi_i \geqslant 30$, and φ_i and ψ_i are reset by Eq. (12):

$$\begin{aligned} \varphi_i &\leftarrow c_i, \\ \psi_i &\leftarrow \psi_i + d_i. \end{aligned} \tag{12}$$

In Eqs. (11) and (12), φ_i is the membrane potential of the i-th neuron, ψ_i is the recovery variable of the i-th neuron, I_i is the external input to the i-th neuron, ξ is internal noise, which is random numbers, generated from a standard normal distribution, that is, $\xi \sim \mathcal{N}(0, \sigma^2)$, where σ is the standard

TABLE I. Parameter sets in Eqs. (11) and (12). (a) Bidirectional coupling case, (b) unidirectional coupling case, and (c) noncoupling case.

Cases	a_1	a_2	b_1	b_2	c_1	c_2	d_1	d_2	I_1	I_2	λ_{12}	λ_{21}
(a)	0.03	0.03	0.3	0.3	−55	−55	2	2	10	10	0.06	0.06
(b)	0.2	0.2	2	2	−56	−56	−16	−16	−99	−99	0	0.02
(c)	0.02	0.0201	0.498	0.499	−47.6	−47.5	2	2.01	10	10	0	0

deviation of the distribution, and a_i and b_i are the parameters of the i-th neuron. In Eq. (12), c_i is the reset value of φ_i, and $\psi_i + d_i$ is the reset value of ψ_i. Furthermore, M is the number of neurons and λ_{ij} is the coupling strength from neuron j to neuron i. The differential equation Eq. (11) is numerically solved by the fourth-order Runge-Kutta method, setting the step size to 0.01.

In the experiments, we set M to two and used three parameter sets: (a) bidirectional coupling, (b) unidirectional coupling, and (c) noncoupling. The values of the parameters we used in Eqs. (11) and (12) are listed in Table I. The coupling forms of two neurons are illustrated in Fig. 5. The red arrows represent the couplings for which a causal relationship exists, and the dotted arrows are the couplings for which a causal relationship does not exist. In the two-neuron experiments, we set ξ to zero in Eq. (11), that is, the spike trains were completely deterministic. When reconstructing an attractor from the observed ISI time series, we set the reconstruction dimension D and time-delay τ to $D = 5$ and $\tau = 1$, respectively. The results of applying the proposed method to spike trains are presented in Fig. 6. In Fig. 6, the horizontal axes represent the length of the ISI time series used in the proposed method, and the vertical axes represent the prediction accuracy of the ISI time series. Furthermore, $\rho[T_i|T_j]$ is the prediction accuracy of T_i by using T_j. In this paper, we refer to the twin surrogate data generated from the ISI time series as twin surrogate ISI (TS-ISI) time series. Namely, T_i^s $(1 \leqslant s \leqslant L)$ is the s-th TS-ISI time series generated from T_i, where L is the number of twin surrogate data. $\rho[T_i^s|T_j]$ $(1 \leqslant s \leqslant L)$ is the prediction accuracy of T_i^s obtained by using T_j, and $\rho'[T_i^s|T_j]$ is the range from the minimum value to the maximum value for all $\rho[T_i^s|T_j]$.

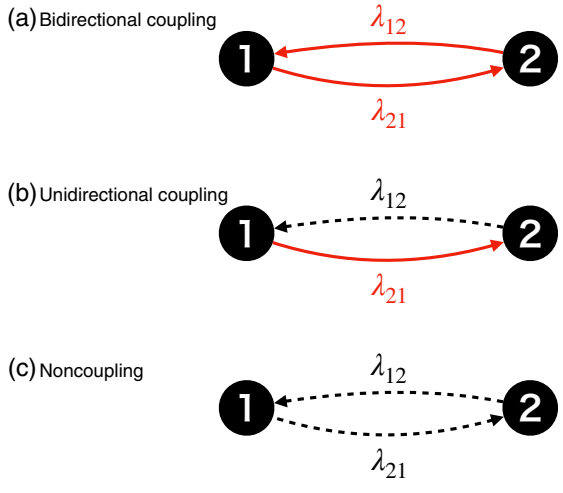


FIG. 5. Coupling forms of two neurons.

We adopted the Monte Carlo method for hypothesis testing [36]. In the Monte Carlo method for hypothesis testing with surrogate data, if statistics calculated by the original data are not included in the range from the minimum to the maximum statistics calculated from surrogate data, the null hypothesis is rejected and the alternative hypothesis is adopted. On the other hand, if statistics calculated by the original data are included in the range from the minimum to the maximum statistics calculated from surrogate data, the null hypothesis is not rejected. Thus, in this study, we compare the prediction accuracy of the original data with the range from the minimum to the maximum prediction accuracies obtained by the twin surrogate data. In this experiment, we set $L = 99$ to ensure that the significance level on the test, denoted by α, satisfies $\alpha = 0.02$, which is obtained from $\alpha = \frac{2}{L+1}$. Consequently, for sufficiently long ISI time series, if the prediction accuracy of T_i by using T_j exceeds the maximum prediction accuracy obtained from all T_i^s $(1 \leqslant s \leqslant L)$ by using T_j, we could reject the null hypothesis (H_0: There is no causality from neuron i to neuron j). In that case, the alternative hypothesis (H_1: There is causality from neuron i to neuron j) could be adopted [36].

As shown in Fig. 6(a), both $\rho[T_1|T_2]$ and $\rho[T_2|T_1]$ converge to approximately $0.5 \sim 0.7$ and exceed the maximum values of $\rho'[T_1^s|T_2]$ and $\rho'[T_2^s|T_1]$ when the ISI time series length is 5000. This finding verifies that we could detect given bidirectional couplings accurately. In Fig. 6(b), $\rho[T_1|T_2]$ exceeds $\rho'[T_1^s|T_2]$; however, $\rho[T_2|T_1]$ is contained within $\rho'[T_2^s|T_1]$ when the ISI time series length is 5000. This result suggests that we could accurately detect unidirectional coupling from neuron 1 to neuron 2. Finally, from Fig. 6(c), it can be seen that both $\rho[T_1|T_2]$ and $\rho[T_2|T_1]$ are contained within $\rho'[T_1^s|T_2]$ and $\rho'[T_2^s|T_1]$ when the ISI time series length is 5000. We conclude that we could accurately detect that causality does not exist when the proposed method was applied to two spike trains.

When applying the proposed method to real-world data, the shorter the required data length, the higher the applicability. Thus, to reveal the required data length for detecting causality, we conducted experiments by varying the ISI time series length in increments of 100 in the range [100, 1000] under the same conditions as Fig. 6 (see Sec. I in Supplemental Material [33]). Moreover, we often observe spike trains with large differences in firing rates and detect causal relationships between them. In other words, it is important to clarify the limitations of applying the proposed method to spike trains with large differences in firing rates. Thus, we evaluated the performance of the proposed method for spike trains with larger differences in firing rates and demonstrate its limitations (see Sec. II in Supplemental Material [33]).

We further investigated the effectiveness of the proposed method in the detection of causality for three neurons. In

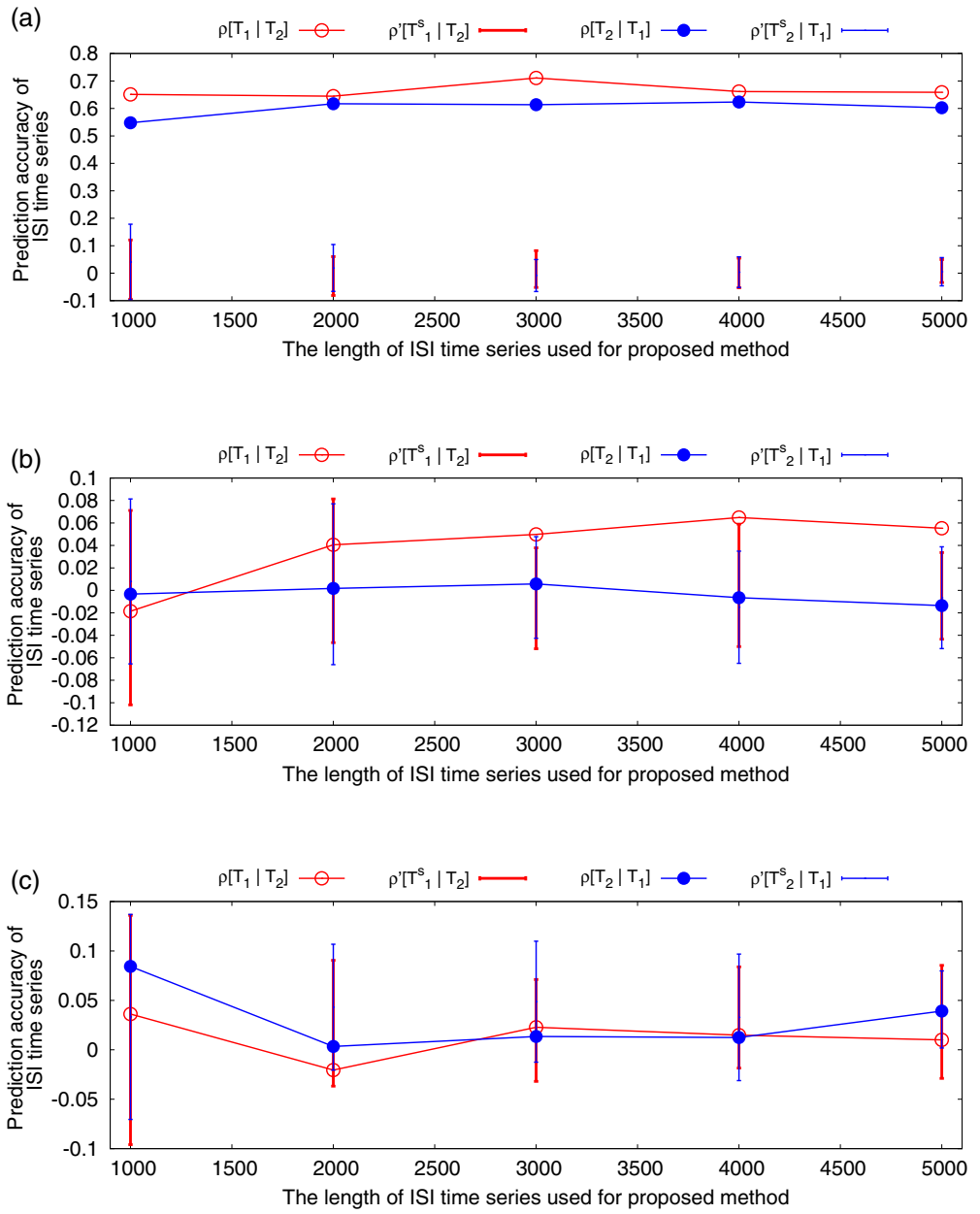


FIG. 6. Results of applying the proposed method to two spike trains. (a) Bidirectional coupling case, (b) unidirectional coupling case, and (c) noncoupling case. Results are evaluated by the prediction accuracy of T_i by using T_j, $\rho[T_i|T_j]$. The error bars of $\rho'[T_i^s|T_j]$ are the ranges from the minimum value to the maximum value for all $\rho[T_i^s|T_j]$ $(1 \leqslant s \leqslant L)$.

Eqs. (11) and (12), we set the value of M to three; the parameter values used in this experiment are listed in Table II. We selected and used parameter values for which the spike train behaved chaotically, as well as their perturbed parameter values. Furthermore, we set the standard deviation, σ, for the normal distribution of random numbers to unity—that is, the noise was drawn from $\mathcal{N}(0, 1)$—because real neurons display noise-based fluctuations. The coupling forms of the three neurons are shown in Fig. 7.

In Fig. 7, the red arrows denote the couplings for which a causal relationship exists, and the dotted arrows denote the couplings for which a causal relationship

TABLE II. Parameter sets used in Eqs. (11) and (12) for the experiment involving the three neurons $(1 \leqslant i \leqslant 3)$, where all λ_{ij} $(1 \leqslant i, j \leqslant 3)$ except λ_{21} and λ_{31} are zero.

a_1	a_2	a_3	b_1	b_2	b_3	c_1	c_2	c_3	d_1	d_2	d_3	I_1	I_2	I_3	λ_{21}	λ_{31}
0.2	0.199	0.198	2	1.99	1.98	−56	−55	−54	−16	−16.1	−16.2	−99	−99.2	−99.4	0.05	0.05

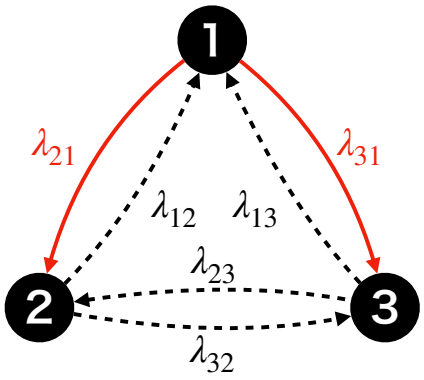


FIG. 7. Coupling forms of three neurons.

does not exist. When reconstructing an attractor from the observed ISI time series, we set the reconstruction dimension D and time-delay τ to $D = 5$ and $\tau = 1$, respectively.

The results of applying the proposed method to three spike trains are presented in Fig. 8. In Fig. 8, the horizontal and vertical axes denote the same values as those in Fig. 6. Figures 8(a)–8(f) display the results of the comparison between the prediction accuracies for the ISI time series of the original spike trains and their corresponding TS-ISI time series. Points of $\rho[T_i|T_j]$ $(1 \leqslant i,\ j \leqslant 3,\ i \neq j)$ represent prediction accuracies of T_i by using T_j. Error bars of $\rho'[T_i^s|T_j]$ $(1 \leqslant i,\ j \leqslant 3,\ i \neq j)$ represent the ranges from the minimum to the maximum prediction accuracies of 234 TS-ISI time series T_i^s by using T_j. In Figs. 8(a) and 8(b), the prediction accuracies $\rho[T_1|T_2]$ and $\rho[T_1|T_3]$ are higher than the maximum values of the prediction accuracies for TS-ISI time series, that is, $\rho[T_1|T_2]$ and $\rho[T_1|T_3]$ are not included in the ranges of $\rho'[T_1^s|T_2]$ and $\rho'[T_1^s|T_3]$ values when the length of the ISI time series is 5000. Therefore, causalities from neuron 1 to neurons 2 and 3 could be accurately detected. On the other hand, in Figs. 8(c)–8(f), the prediction accuracies of the original ISI time series are included in the ranges from the minimum to the maximum prediction accuracies of the TS-ISI time series, thus we could accurately detect no causalities from neuron 2 to neurons 1 and 3, and from neuron 3 to neurons 1 and 2. From these results, we could detect the given causality from neuron 1 to neurons 2 and 3 (see Sec. IV in Supplemental Material [33] text for other cases).

The reason that we generated 234 surrogate data to test for causality is due to the multiple testing problem. In the case of three neurons, we need to perform the causality tests for

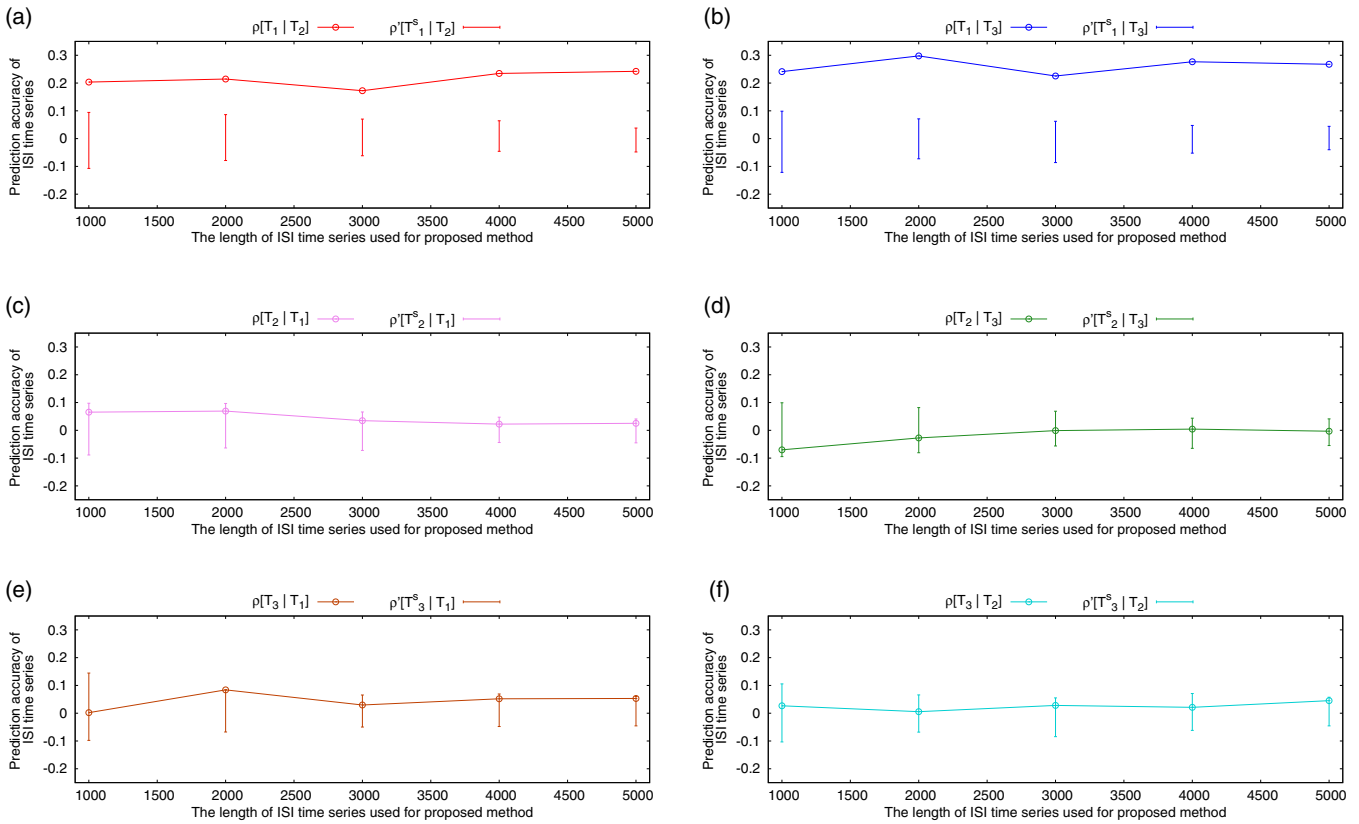


FIG. 8. Results of applying the proposed method to three spike trains. Each panel shows the comparison results between the prediction accuracies for the ISI time series of the original spike train and its corresponding TS-ISI time series generated by the twin surrogate method. Points and lines about $\rho[T_i|T_j]$ $(1 \leqslant i,\ j \leqslant 3,\ i \neq j)$ represent prediction accuracies of T_i by using T_j. Error bars about $\rho'[T_i^s|T_j]$ $(1 \leqslant i,\ j \leqslant 3,\ i \neq j)$ represent the ranges from the minimum to the maximum values of prediction accuracies for TS-ISI time series, T_i^s by using T_j where we obtained $\rho'[T_i^s|T_j]$ from 234 TS-ISI time series. The results of detecting causality (a) from neuron 1 to neuron 2 $(1 \to 2)$, (b) from neuron 1 to neuron 3 $(1 \to 3)$, (c) from neuron 2 to neuron 1 $(2 \to 1)$, (d) from neuron 2 to neuron 3 $(2 \to 3)$, (e) from neuron 3 to neuron 1 $(3 \to 1)$, and (f) from neuron 3 to neuron 2 $(3 \to 2)$.

six cases ($1 \to 2,\ 2 \to 1,\ 1 \to 3,\ 3 \to 1,\ 2 \to 3,\ 3 \to 2$). Thus, when estimating the network structure, the significance level for the single test needs to be adjusted based on the multiplicity of the tests to obtain the appropriate significance level for multiple tests. In multiple testing, there are several ways to adjust the significance level depending on the conditions. One of the simplest ways to calculate the significance level for multiple testing is the Šidák correction [37], which is $\alpha_m = 1 - (1 - \alpha_s)^z$, where α_m is the significance level for multiple testing, α_s is the significance level for single testing, and z is the number of tests. If we set α_m to 0.05 when testing six times ($z = 6$), we obtain $\alpha_s = 1 - \sqrt[6]{0.95} (\approx 0.008513)$ by solving the following equation: $0.95 = (1 - \alpha_s)^6$. In addition, when adopting the Monte Carlo method for hypothesis testing, α_s and the number of surrogate data L should satisfy the following equation: $(L + 1)\frac{\alpha_s}{2} = 1$. From this equation, we obtained the number of surrogate data L; $L = \frac{2}{\alpha_s} - 1 = \frac{2}{1 - \sqrt[6]{0.95}} - 1 = 233.95 \cdots \approx 234$.

IV. CONCLUSIONS

This study proposed a method for detecting causality in spike trains by modifying the original CCM method. To this end, two modification techniques, namely the technique of state space reconstruction from ISIs and the technique of establishing the temporal correspondence of two ISI time series, were incorporated into the CCM procedure. Numerical experiments demonstrated that the proposed method could detect causality for two or three spike trains. Therefore, this study demonstrated the applicability of CCM to spike trains by modifying the original CCM method to the ISI time series based on spike timing. Moreover, it is important to use TS data for testing in causality detection. Although the ranges of prediction accuracy displayed in Figs. 6 and 8 are not high, the presence of causality was detected accurately by comparing the ranges of the prediction accuracy values of TS data.

A limitation of the proposed method is that the target systems for detecting causality are nonlinear deterministic dynamical systems. That is, the proposed method is not effective for fully stochastic spike trains. However, the experiments of three neurons confirmed that the proposed method works well for nonlinear deterministic systems with internal noise drawn from a normal distribution. Although the results show that the proposed method is effective for a model of coupled neurons with weak internal noise, we will evaluate the robustness of the proposed method for general nonlinear dynamical systems with strong internal noise in future work. In addition, the proposed method is not effective for periodic spike trains and synchronized spike trains, because it may be able to make predictions despite the absence of causality, and the prediction accuracy remains unchanged with increasing volume of data. The above-mentioned limitations of the proposed method for stochastic, periodic, and synchronized spike trains were derived from the original CCM, corresponding to its potential application limits. Thus, it is important to develop a method of detecting causality for fully stochastic dynamical systems in future studies.

Moreover, we often observe nonstationary spike trains. When applying the proposed method to nonstationary spike trains, by considering the difference of ISI time series: $T_d(n) = T(n + 1) - T(n)$, we can eliminate the nonstationarity and obtain a stationary time series $T_d(n)$ from nonstationary ISI time series $T(n)$ [38]. Note that $T(n)$ is required to be a unit root process, i.e., $T(n)$ is nonstationary and $T_d(n)$ is stationary. Through this preprocessing, it may be possible to detect causality by the proposed method, which is an important future work.

This study demonstrated the detection of causality for only two or three neurons. However, we have shown that prediction accuracies obtained using the original CCM framework become low values when the number of connected elements in a system is increased [4]. Thus, the coupling estimation for large networks remains a challenging task and is also a latent problem in many other causality detection methods based on prediction accuracy [4,6–8]. Future works will focus on solving these problems and achieving coupling estimation only from spike trains for larger networks. The estimation of global information flows based on network theory, in addition to local one-to-one mutual predictions, will be a critical breakthrough.

ACKNOWLEDGMENTS

This study was supported by JSPS KAKENHI Grants No. JP22J14621, No. JP22KJ2815, and No. JP24K23902 for K.S., JSPS KAKENHI Grants No. JP20H00596, No. JP21H03514, No. JP21H03508, No. JP21K12093, No. JP22K18419, No. JP23K21706, No. JP23K21701, No. JP23K04274, No. JP24K03013, No. JP25K03192, and No. JP25H00447 for Y.S., and JSPS KAKENHI Grants No. JP20H00596, No. JP21H03514, No. JP22K18419, No. JP23K21706, No. JP25K03189, and No. JP25H00447 for T.I.

[1] S. K. Stavroglou, A. A. Pantelous, H. E. Stanley, and K. M. Zuev, Hidden interactions in financial markets, Proc. Natl. Acad. Sci. USA **116**, 10646 (2019).

[2] Y. Hirata, J. M. Amigó, Y. Matsuzaka, R. Yokota, H. Mushiake, and K. Aihara, Detecting causality by combined use of multiple methods: Climate and brain examples, PLoS One **11**, e0158572 (2016).

[3] H. Ma, K. Aihara, and L. Chen, Detecting causality from nonlinear dynamics with short-term time series, Sci. Rep. **4**, 7464 (2014).

[4] K. Sawada, Y. Shimada, and T. Ikeguchi, Network structure detection using convergent cross mapping on multivariate time series, Nonlinear Theory Appl. IEICE **11**, 422 (2020).

[5] R. A. García, A. C. Martí, C. Cabeza, and N. Rubido, Small-worldness favours network inference in synthetic neural networks, Sci. Rep. **10**, 2296 (2020).

[6] C. W. J. Granger, Investigating causal relations by econometric models and cross-spectral methods, Econometrica: J. Econom. Soc. **37**, 424 (1969).

[7] T. Schreiber, Measuring information transfer, Phys. Rev. Lett. **85**, 461 (2000).
[8] G. Sugihara, R. May, H. Ye, C.-H. Hsieh, E. Deyle, M. Fogarty, and S. Munch, Detecting causality in complex ecosystems, Science **338**, 496 (2012).
[9] F. Takens, Detecting strange attractors in turbulence, in *Dynamical Systems and Turbulence*, Lecture Notes in Mathematics, edited by D. Rand and L. Young (Springer-Verlag, Berlin, Heidelberg, 1981), Vol. 898, pp. 366–381.
[10] T. Sauer, J. A. Yorke, and M. Casdagli, Embedology, J. Stat. Phys. **65**, 579 (1991).
[11] S. Leng, H. Ma, J. Kurths, Y.-C. Lai, W. Lin, K. Aihara, and L. Chen, Partial cross mapping eliminates indirect causal influences, Nat. Commun. **11**, 2632 (2020).
[12] H. Suzuki, K. Aihara, J. Murakami, and T. Shimozawa, Analysis of neural spike trains with interspike interval reconstruction, Biol. Cybern. **82**, 305 (2000).
[13] L. Telesca and M. Lovallo, Analysis of seismic sequences by using the method of visibility graph, Europhys. Lett. **97**, 50002 (2012).
[14] H. Pratiwi, L. S. Rini, and I. W. Mangku, Marked point process for modelling seismic activity (case study in sumatra and java), J. Phys.: Conf. Ser. **1022**, 012004 (2018).
[15] Y. Hirata and K. Aihara, Timing matters in foreign exchange markets, Physica A **391**, 760 (2012).
[16] J. Runge, V. Petoukhov, and J. Kurths, Quantifying the strength and delay of climatic interactions: The ambiguities of cross correlation and a novel measure based on graphical models, J. Clim. **27**, 720 (2014).
[17] J. Runge, V. Petoukhov, J. F. Donges, J. Hlinka, N. Jajcay, M. Vejmelka, D. Hartman, N. Marwan, M. Paluš, and J. Kurths, Identifying causal gateways and mediators in complex spatio-temporal systems, Nat. Commun. **6**, 8502 (2015).
[18] S. Gupta, Z. Su, N. Boers, J. Kurths, N. Marwan, and F. Pappenberger, Interconnection between the Indian and the East Asian summer monsoon: Spatial synchronization patterns of extreme rainfall events, Int. J. Climatol. **43**, 1034 (2023).
[19] K. Kuroda, T. Ashizawa, and T. Ikeguchi, Estimation of network structures only from spike sequences, Physica A **390**, 4002 (2011).
[20] K. Kuroda, K. Fujiwara, and T. Ikeguchi, Identification of neural network structure from multiple spike sequences, in *Neural Information Processing*, Lecture Notes in Computer Science, edited by T. Huang, Z. Zeng, C. Li, and C. S. Leung (Springer, Berlin, Heidelberg, 2012), Vol. 7664, pp. 184–191.
[21] K. Kuroda, H. Hashiguchi, K. Fujiwara, and T. Ikeguchi, Reconstruction of network structures from marked point processes using multi-dimensional scaling, Physica A **415**, 194 (2014).
[22] K. Kuroda and M. Hasegawa, Method for estimating neural network topology based on SPIKE-distance, in *Artificial Neural Networks and Machine Learning–ICANN 2016*, Lecture Notes in Computer Science, edited by A. Villa, P. Masulli, and A. P. Rivero (Springer, Cham, 2016), Vol. 9886, pp. 91–98.
[23] R. Kobayashi, S. Kurita, A. Kurth, K. Kitano, K. Mizuseki, M. Diesmann, B. J. Richmond, and S. Shinomoto, Reconstructing neuronal circuitry from parallel spike trains, Nat. Commun. **10**, 4468 (2019).
[24] T. Sauer, Reconstruction of dynamical systems from interspike intervals, Phys. Rev. Lett. **72**, 3811 (1994).
[25] T. Sauer, Interspike interval embedding of chaotic signals, Chaos **5**, 127 (1995).
[26] J. P. Huke and D. S. Broomhead, Embedding theorems for non-uniformly sampled dynamical systems, Nonlinearity **20**, 2205 (2007).
[27] T. Sauer, Reconstruction of integrate-and-fire dynamics, in *Nonlinear Dynamics and Time Series: Building a Bridge Between the Natural and Statistical Sciences*, edited by C. D. Cutler and D. T. Kaplan (AMS Fields Institute Communications, 1997), Vol. 11, pp. 63–75.
[28] M. Thiel, M. C. Romano, J. Kurths, M. Rolfs, and R. Kliegl, Twin surrogates to test for complex synchronisation, Europhys. Lett. **75**, 535 (2006).
[29] S.-I. Nakayama, A. Takasuka, M. Ichinokawa, and H. Okamura, Climate change and interspecific interactions drive species alternations between anchovy and sardine in the western north pacific: detection of causality by convergent cross mapping, Fish. Oceanogr. **27**, 312 (2018).
[30] J.-P. Eckmann, S. O. Kamphorst, and D. Ruelle, Recurrence plots of dynamical systems, Europhys. Lett. **4**, 973 (1987).
[31] N. Marwan, M. C. Romano, M. Thiel, and J. Kurths, Recurrence plots for the analysis of complex systems, Phys. Rep. **438**, 237 (2007).
[32] G. Lancaster, D. Iatsenko, A. Pidde, V. Ticcinelli, and A. Stefanovska, Surrogate data for hypothesis testing of physical systems, Phys. Rep. **748**, 1 (2018).
[33] See Supplemental Material at http://link.aps.org/supplemental/10.1103/t2jb-vvx9 for supplementary consideration, experiments, and figures.
[34] E. M. Izhikevich, Simple model of spiking neurons, IEEE Trans. Neural Networks **14**, 1569 (2003).
[35] K. Naiki, Y. Shimada, K. Fujiwara, and T. Ikeguchi, Chaotic responses and chaos synchronization in Izhikevich neuron model, IEICE Trans. Fundam. Electron. Commun. Comput. Sci. **J100-A**, 195 (2017) (in Japanese).
[36] J. Theiler and D. Prichard, Constrained-realization Monte Carlo method for hypothesis testing, Physica D **94**, 221 (1996).
[37] Z. Šidák, Rectangular confidence regions for the means of multivariate normal distributions, J. Am. Stat. Assoc. **62**, 626 (1967).
[38] R. Salles, K. Belloze, F. Porto, P. H. Gonzalez, and E. Ogasawara, Nonstationary time series transformation methods: An experimental review, Knowledge Based Syst. **164**, 274 (2019).